MARCH 2017 VOLUME 2 NUMBER 3 pubs.acs.org/acssensors

ACS SENSORS

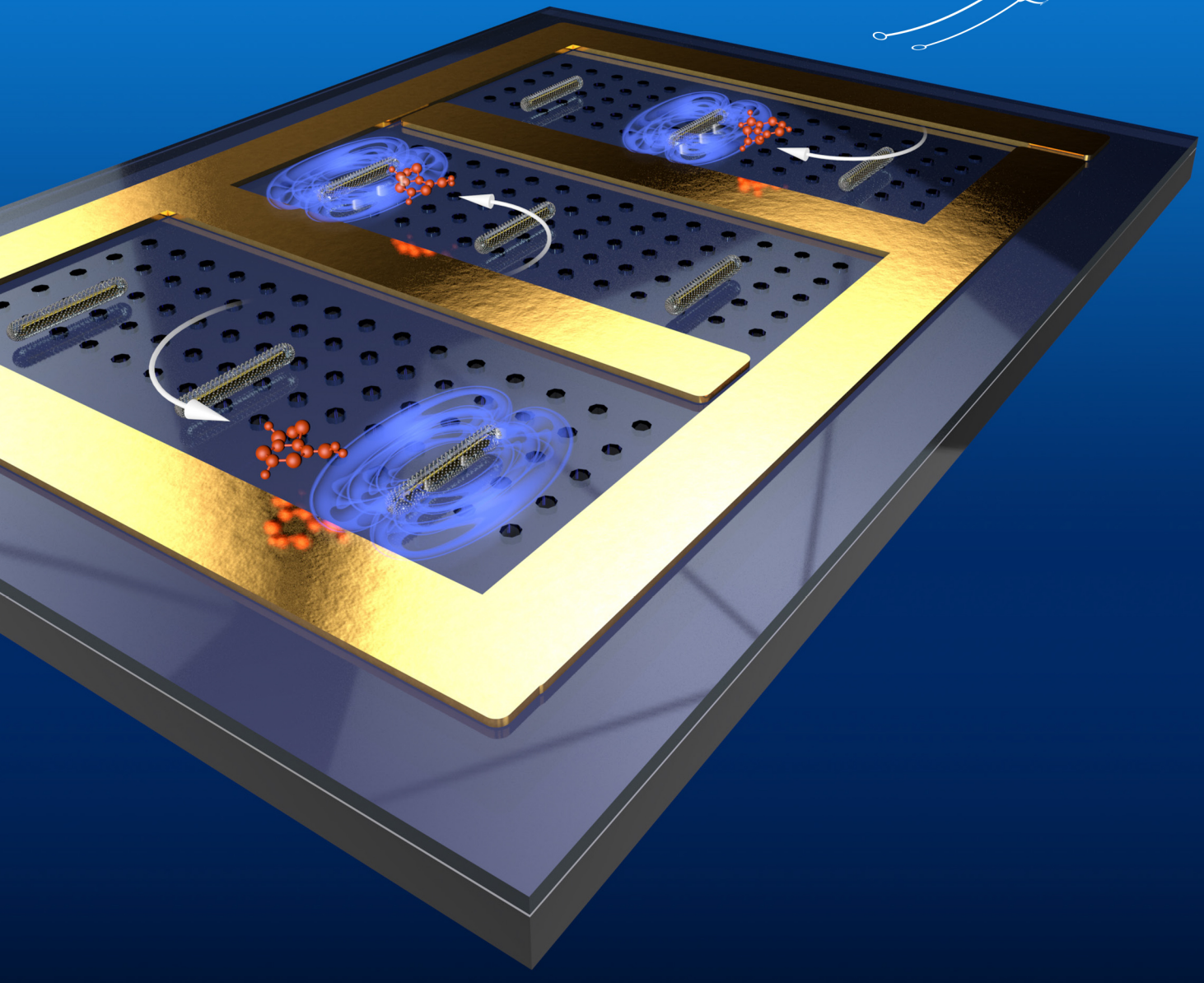

ACS Publications
Most Trusted. Most Cited. Most Read.

www.acs.org

ACS SENSORS

Article

pubs.acs.org/acssensors

Electrokinetic Manipulation Integrated Plasmonic–Photonic Hybrid Raman Nanosensors with Dually Enhanced Sensitivity

Chao Liu,[†,¶] Zheng Wang,[†,‡,¶] Erwen Li,[§] Zexi Liang,[†] Swapnajit Chakravarty,[∥] Xiaochuan Xu,[∥] Alan X. Wang,[*,§] Ray T. Chen,[*,†,‡] and Donglei Fan[*,†,⊥,#]

[†]Materials Science and Engineering Program, Texas Materials Institute and [⊥]Department of Mechanical Engineering, The University of Texas at Austin, Austin, Texas 78712, United States

[‡]Department of Electrical and Computer Engineering, The University of Texas at Austin, 10100 Burnet Road, MER 160, Austin, Texas 78758, United States

[§]School of Electrical Engineering and Computer Science, Oregon State University, Corvallis, Oregon 97331, United States

[∥]Omega Optics, Inc., 8500 Shoal Creek Boulevard, Building 4, Suite 200, Austin, Texas 78757, United States

[#]Nova Minds LLC, 9535 Ketona Cv., Austin, Texas 78759, United States

Supporting Information

ABSTRACT: To detect biochemicals with ultrahigh sensitivity, efficiency, reproducibility, and specificity has been the holy grail in the development of nanosensors. In this work, we report an innovative type of photonic–plasmonic hybrid Raman nanosensor integrated with electrokinetic manipulation by rational design, which offers dual mechanisms that enhance the sensitivity for molecule detection directly in solution. For the first time, we integrate large arrays of synthesized plasmonic nanocapsules with densely surface distributed silver (Ag) nanoparticles (NPs) on lithographically patterned photonic crystal slabs via electric-field assembling. With the interdigital microelectrodes, the applied electric fields not only assemble the hybrid plasmonic nanocapsules on photonic crystal slabs, but also generate electrokinetic flows that focus analyte molecules to the Ag hot spots on the nanocapsules for surface-enhanced Raman scattering (SERS) detection. The synergistic effects of plasmonic–photonic resonance and the electrokinetic molecular focusing can promote the SERS enhancement factor (EF) robustly to ~2×10^9. Various molecules including SERS probing molecules, nucleobases, and unsafe food additives can be detected directly from suspension. The innovative mechanism, design, and fabrication reported in this work can inspire a new paradigm for achieving high-performance Raman nanosensors, which is pivotal for lab-on-chip disease diagnosis and environmental protection.

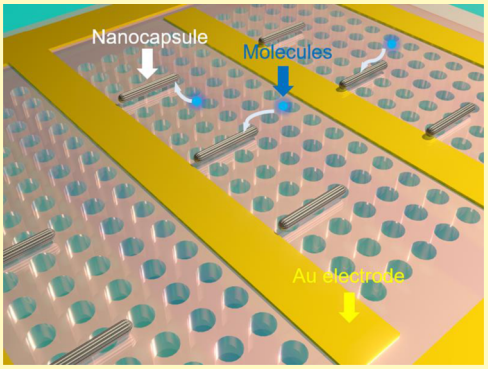

KEYWORDS: *surface-enhanced Raman scattering, photonic crystal, guided-mode resonance, electrokinetic manipulation, Raman nanosensor*

The holy grail in the development of biochemical nanosensors is to obtain ultrahigh sensitivity, efficiency, reproducibility, and specificity in molecule detection. Among various sensing mechanisms, surface-enhanced Raman scattering (SERS), which utilizes localized surface plasmon resonance (LSPR) to obtain ultrahigh enhancement of Raman signals of molecules, is one of the most promising techniques, which can offer advantageous label-free and multiplex detection. With rational designs, reports show that some SERS substrates can enhance Raman signals of molecules to 10^{10}, which can readily detect single molecules of various species.[1−3] Applications of SERS have been demonstrated, ranging from diagnosis of prestage diseases,[4−7] detection of warfare agents,[8−11] to environmental protection.[12−16] However, the practical applications of SERS are still hindered by a few hurdles. First, it remains challenging to obtain SERS substrates with robust ultrahigh enhancement. Second, it requires great effort to fabricate/assemble plasmonic nanoparticles (NPs)/substrates at designated locations for position deterministic detection. Third, most SERS detections are performed in a dried environment so that target molecules during the drying process can be forced to attach to SERS substrates, where ultrahigh enhancement only exists in a region of tens of nanometers near the SERS substrates.[17−19] It is highly desirable to detect molecules directly from solution to study SERS effects since the drying process of analytes can have the "coffee ring effect",[20,21] which makes the obtained results depend on individuals and groups. However, when directly detecting from suspension, it is arduous to focus interesting molecules on the surface of SERS

Received: September 18, 2016
Accepted: January 30, 2017
Published: January 30, 2017

DOI: 10.1021/acssensors.6b00586
ACS Sens. 2017, 2, 346−353

nanosensors. New mechanisms must be considered to overcome the issue.

Recently, guided-mode resonance (GMR) in photonic crystal slabs (PCSs), which has been extensively studied in filter applications,[22−25] has drawn great attention for its potential application in the enhancement of Raman signals. Guided-mode resonance can substantially boost localized electric fields (E) in the vicinity of PCSs due to their efficient trapping of the light. The effect can readily enhance Raman signals of molecules due to the E^4 dependence.[18,19,26] Noticeably, the mechanism of Raman enhancement by GMR is similar to that of LSPR. It is intriguing that even higher EF can be obtained by coupling GMR with LSPR. Recently, a few research groups including us have demonstrated coupling of the GMR with LSPR from metallic NPs for enhanced Raman detection.[27−29] However, none of the existing articles have offered the capability in instant assembly and alignment of plasmonic NPs at designated positions on PCSs, not to mention active focusing of molecules in solution for direct sensing on PCSs.

In this work, we report an integrated lab-on-a-chip system which for the first time offers two enhancement mechanisms that improve both sensitivity and efficiency in SERS detection directly from solution. The device is made of bottom-up synthesized SERS nanocapsules and top-down fabricated PCSs. The SERS-active nanocapsules are efficiently assembled on top of PCSs and form aligned arrays by electric fields. The synergistic resonance of PCSs and plasmonic NPs can effectively enhance SERS detection. The applied electric field via integrated microelectrodes not only assembles nanocapsules but also effectively attracts analyte molecules to the plasmonic nanocapsules to increase the concentration and interaction of molecules with the high-density plasmonic hot spots on the surface of nanocapsules. As a result, the device can improve the detection sensitivity and efficiency directly from liquid suspension in a rational and designed manner. Experiments show that in addition to the high Raman enhancement of ∼3.7 × 10^8 from the plasmonic nanocapsules, the designed PCS provides another 3 times enhancement. Furthermore, with optimized ac frequencies and voltages, analyte molecules, including Nile blue, adenine, and melamine, can be effectively concentrated on the surface of the nanocapsules, which further increases the enhancement by 19% to 45%. In total, the designed structures can robustly improve the detection sensitivity by an additional 5 times on top of the existing SERS enhancement of 3.7 × 10^8. The device could be readily integrated with microfluidics for on-chip molecule sensing by Raman spectroscopy.

The electrokinetic manipulation integrated plasmonic−photonic hybrid nanosensors consist of three components: (1) chemically synthesized plasmonic nanocapsules, where billions of NPs can be fabricated on the outermost surface of the nanocapsules at a time; (2) PCSs with a square lattice of circular nanoholes are fabricated via electron-beam lithography (EBL) and dry etching; and (3) interdigital microelectrodes patterned on the PCSs via the common photolithography based lift-off process (Figure 1a). Here, each component serves a purpose: the nanocapsules, with a metallic gold (Au) nanorod core and dense silver (Ag) NPs on the outer surface, can be readily maneuvered into aligned arrays in an external electric field and provide ultrahigh sensitivity for SERS detection (Figure 1b and Figure 2a−c); the PCSs are carefully designed to match its resonance with the excitation laser wavelength (633 nm randomly polarized laser, Research Electro-Optics, Inc.) to further boost the SERS sensitivity of the nanocapsules due to the substantially enhanced electromagnetic fields; finally, the patterned microelectrodes on the PCSs provide electric fields to manipulate and assemble the plasmonic nanocapsules as well as to actively focus analyte molecules on the SERS sensitive surface of the nanocapsules, providing additional enhancement in terms of the detection efficiency and sensitivity.

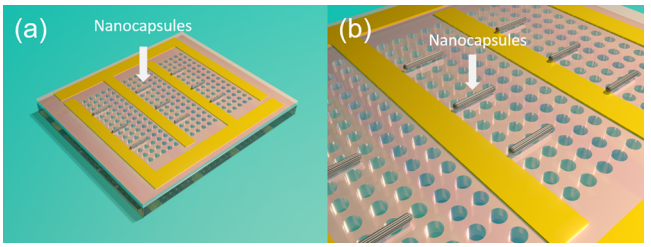

Figure 1. Schematics of electrokinetic manipulation integrated plasmonic−photonic hybrid nanosensor system.

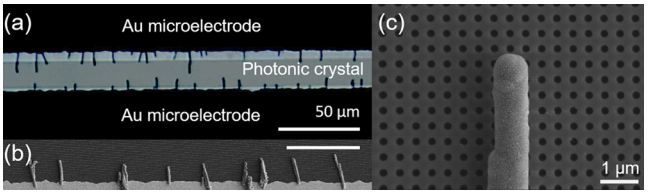

Figure 2. (a) Optical microscopy image of aligned nanocapsules on interdigital microelectrodes with lithographed nanophotonic crystals. AC E-fields are applied on the Au microelectrodes. (b) SEM image of aligned plasmonic nanocapsules after water evaporation. The scale bar is 30 μm. (c) SEM image of a nanocapsule aligned on the PCS via the microelectrodes.

The fabrication of the PCSs with patterned interdigital microelectrodes is via top-down lithography as illustrated in Figure 3a−c. In brief, the fabrication starts with creating a two-

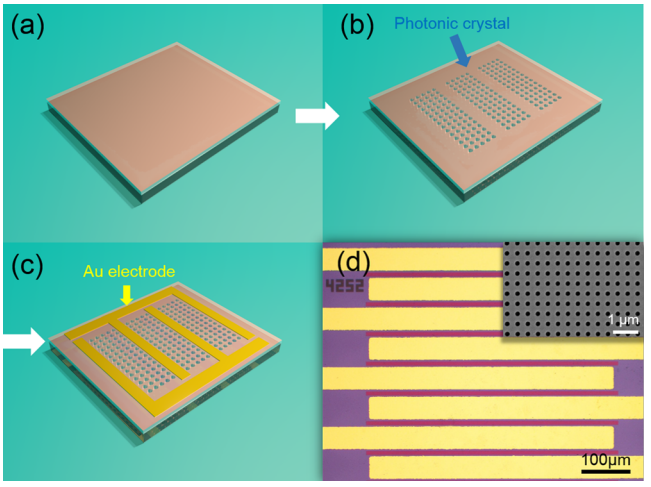

Figure 3. Fabrication schemes of the PCSs with embedded interdigital microelectrodes. (a) Fused silica is coated with a thin layer of Si_3N_4 (thickness: 230 nm). (b) PCSs are fabricated by EBL and RIE. (c) Au interdigital microelectrodes are patterned by photolithography, followed by electron-beam evaporation. (d) Optical microscope image of the obtained PCSs with embedded interdigital electrodes; inset is the enlarged image of the PCS with a = 425 nm and d = 213 nm.

DOI: 10.1021/acssensors.6b00586
ACS Sens. 2017, 2, 346−353

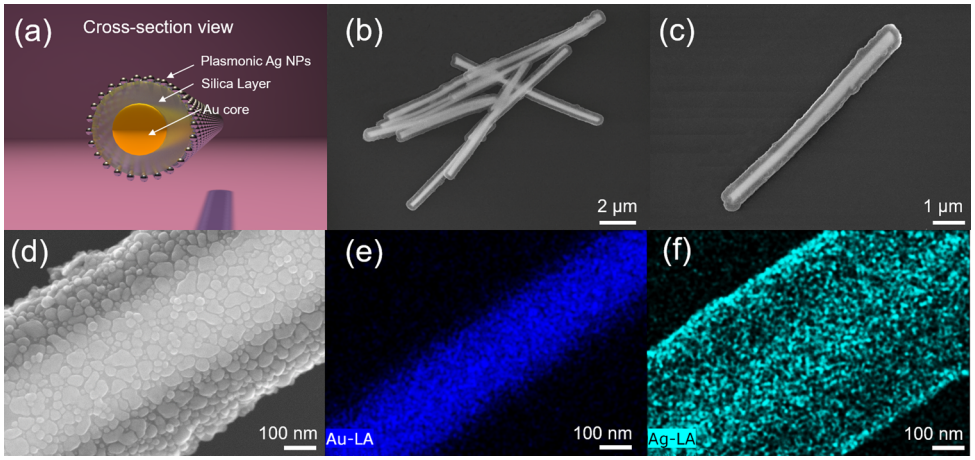

Figure 4. (a) Cross-sectional schematic of a nanocapsule where a metallic Au nanowire serves as the core, a silica layer grown on the surface of the metal core support the Ag NPs growth, and Ag NPs grow uniformly on the silica layer. (b,c) SEM images of nanocapsules, (d) high-density Ag nanoparticles grown on the surface of the nanocapsule. (e,f) EDS mappings of Au and Ag distribution of a nanocapsule, respectively.

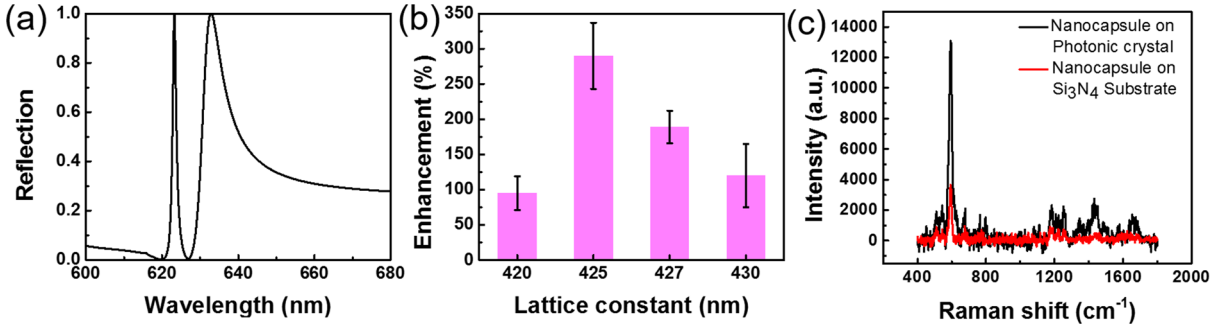

Figure 5. (a) Simulated reflection spectrum of the PCS (a = 425 nm and d = 213 nm). (b) Enhancements of the Raman signals from PCSs with various lattice constant a at the same hole size d. (c) Full Raman spectrum of 100 nm Nile blue detection on the PCS (a = 425 nm and d = 213 nm) and on the flat Si_3N_4 substrate, respectively.

dimensional (2D) ordered arrays of nanoholes on a 230-nm-thick Si_3N_4 film, which is deposited on a fused silica substrate, via EBL followed by reactive ion etching (RIE) (Figure 3b). Next, the substrate is cleaned in piranha solution and Remover PG at 85 °C for 1 h before a set of Au (150 nm)/Cr (10 nm) interdigital microelectrodes is patterned on the PCSs via the common photolithography based lift-off process (Figure 3c,d).

The SERS-active nanocapsules are obtained by chemical synthesis including electrochemical deposition and hydrothermal growth.[30,31] The nanocapsules consist of a trilayer structure with a Au nanorod as the core, a thin silica layer coated on the surface of the Au core, and an outer layer of high-density Ag NPs grown on the silica layer (Figure 4). Energy dispersive spectroscopy (EDS) analysis confirms that the inner core is Au and the outmost surface is covered by Ag (Figure 4e,f). The inner Au nanorod cores are fabricated by electrochemical deposition into nanoporous templates. Billions of nanorods can be made at a time with tunable lengths and diameters.[32] They can be electrically polarized and manipulated in an electric field.[33] The silica layers are synthesized via hydrolysis of tetraethyl orthosilicate (TEOS, 0.8 mL, Alfa Aesar, 99.999+%) in a mixed solution of ammonia (0.2 mL, Fisher Scientific, Certified A.C.S. Plus), ethanol (3 mL, Pharmco-aaper, ACS/USP grade), and deionized water (1.8 mL), which not only provide supporting substrates for the growth of Ag NPs but also effectively separate them from the Au cores to avoid the possible optical quenching effect. The uniform Ag NPs on the silica surface are grown by the reduction of silver nitrate ($AgNO_3$) in polyvinylpyrrolidone (PVP). The size of Ag NPs and their junctions are optimized to 26 ± 5 nm and 1.8 ± 0.4 nm, respectively, which provide an EF of 3.7×10^8 for ultrasensitivity SERS detection[30] (a more detailed calculation of enhancement factor is in Supporting Information). The detailed synthesis procedure is described in the Supporting Information.

Next, the chemically synthesized plasmonic nanocapsules are assembled into arrays on the lithographed PSCs by electric fields created via the interdigital microelectrodes on the PCSs (Figure 2a–c). Upon applying ac voltage of 20 V at 700 kHz, we found the nanocapsules instantly aligned and transported to attach to the edge of the microelectrodes, forming into parallel arrays. The alignment and assembling are due to the dielectrophoretic (DEP) force resulted from the interaction between the electrically polarized nanocapsules and the ac electric field (E), given by $F = p \cdot \nabla E$[34] where p is the electric dipole moment. Owing to the strong polarization of the metallic Au nanorod core, the transportation and assembling can be accomplished in 120 s at 20 V and 700 kHz.[35] These results agree with our previous study that metallic longitudinal nanostructures can be strongly polarized and efficiently transported toward the highest of E-field gradient and aligned with the E-field.[35] Therefore, by exploiting the advanced top-down lithography and field induced assembling techniques, we facilely obtained a new type of plasmonic–photonic hybrid

DOI: 10.1021/acssensors.6b00586
ACS Sens. 2017, 2, 346–353

nanodevices. The design offers dual enhancement of sensitivity for molecule detection that leverage the merits of each type of integrated components: (1) the guided-mode resonance of PCSs can be readily coupled with the excitation laser to promote the plasmonic resonance of the nanocapsules to enhance SERS; (2) the electric field can actively induce enrichment of biochemicals to the plasmonic hot spots on the entire surface of the nanocapsules for efficient and sensitive SERS detection.

To understand and determine the roles of each effect, we conducted a series of numerical simulations and experiments. Guided by rigorous coupled-wave analysis (RCWA), we performed simulations via S4, which is a frequency domain simulator to solve the linear Maxwell's equations in layered periodic structure.[36] Figure 5a shows the simulated reflection spectrum of the PCS, which has a square lattice (the lattice constant a equals 425 nm) of circular nanoholes (the diameter d equals 213 nm). The parameters (a = 425 nm and d = 213 nm) we choose for the PCS are to realize a relatively wide Fano resonance peak centered at the 633 nm excitation wavelength because it could tolerate more fabrication fluctuations, which is essential for fabrication of robust SERS substrate. Considering the possible fabrication errors and overly optimistic simulation, we carried out experiments by fabricating PCSs with different lattice constants of 420, 425, 427, and 430 nm at a fixed hole size of 213 nm (the simulated reflection spectra of the four designs can be found in Supporting Information Figure S1). Then, we dispersed and dried the nanocapsules in a polydimethylsiloxane (PDMS) well attached on the PCSs followed by introducing Nile blue solution (20 μL of 100 nM) in the same PDMS well. The system is sealed with a coverslip. After incubating for 10 min, Raman spectra of Nile blue molecules are taken from the plasmonic–photonic hybrid nanostructures in solution. The enhancements of different PCSs are quantitatively determined by comparing the collected Raman signals of Nile blue on the nanocapsules-on-photonic crystals to that of the control experiment from nanocapsules on a flat Si_3N_4 substrate (Figure 5c). To ensure the rigidity of the experiments, for each type of samples, at least five spectra were obtained and averaged. As expected, the highest average enhancement of ~300% is obtained from the PCS with a lattice constant of 425 nm and hole size of 213 nm, which is shown in Figure 5b. To further quantitatively evaluate this nanocapsules-on-PCS system, we carried out a numerical simulation of a nanocapsule placed on top of a PCS in water environment using FullWAVE module of Rsoft photonic component design suite based on three-dimensional (3D) finite-difference time-domain (FDTD) algorithm. Figure 6a illustrates the schematic of the simulated structure. The nanocapsule is modeled as a trilayer concentric cylinder. The Au nanowire (300 nm in diameter) in the center is surrounded by a silica coating layer (180 nm thick). Outside of that, there is a layer of randomly distributed Ag NPs (26 nm in diameter), and the minimum gap between Ag NPs is 5 nm, which is slightly larger than the real synthesized nanostructures' gap size, an average of 1.8 nm. Here, 5 nm is chosen in the simulation to reduce the requirement of minimum FDTD simulation grid size. The nanocapsule is placed on top of the PCS, which consists of a Si_3N_4 layer (230 nm thick) with the square lattice (a = 425 nm) of nanoholes (d = 213 nm, filled with water) on top of a silica substrate. The incident light is a 633 nm Gaussian beam with a beam diameter of 2.5 μm. Because the SERS enhancement factor (EF) is proportional to the fourth power of

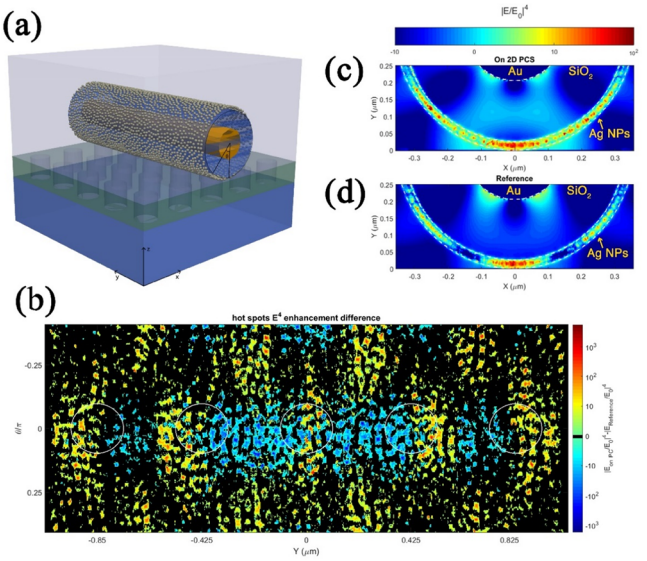

Figure 6. (a) Schematic of the simulated structure using FullWAVE module of Rsoft photonic component design suite based on the 3D FDTD method. (c) and (d) show the E^4 enhancement distribution after averaging along the nanowire direction on the PCS (a = 425 nm and d = 213 nm) and a flat Si_3N_4 (230 nm thick) coated silica substrate, respectively. The white dashed lines represent the material boundary. (b) Plot of the difference of E^4 enhancement distribution of the Ag NPs layer in the region shown in (c) and (d) where the nanocapsule is placed on the PCS and the flat Si_3N_4 substrate, respectively. Here the cylindrically shaped Ag NPs layer has been mapped to a planar layer. The white circle indicates the position of the holes on the PCS.

the local electric field amplitude, we calculate the E^4 enhancement (defined as $|E/E_0|^4$) to evaluate the SERS EF, where E is the field where the nanocapsule sits on the substrates and E_0 is the peak amplitude of the excitation field in the center of the Gaussian beam. The results are compared to a reference simulation where the same nanocapsule is placed on top of a flat Si_3N_4 (230 nm thick) film coated silica substrate. Panels c and d in Figure 6 show the E^4 enhancement distribution at the cross section of the nanocapsule placed on two different substrates after averaging along the nanowire direction. Clearly, the SERS EF is dominated by the hot spots in the Ag NPs layer. Because the PCS increases the local electric field due to the GMR effect, when the nanocapsule is placed on the PCS, the lower part of the nanocapsule couples with the GMR, which enhances the hot spots in the Ag NPs layer as shown in Figure 6c. Since the GMR is a localized effect, the upper part of the nanocapsule does not show obvious coupling with the PCS. Thus, the enhancement of SERS EF from the upper part of the nanocapsule is negligible, which is not considered in our comparison. Figure 6b plots the difference of E^4 enhancement distribution on the Ag NPs layer between these two cases, in which the cylindrical shaped Ag NPs layer has been mapped to a planar layer. We only plot the hot spots where E^4 enhancement is bigger than 10. The labeled value is averaged along the radial direction (vertical direction after mapping) over the 26 nm Ag NP layer. On the PCS, the hot spots distribution profile is greatly modified and shows a strong correlation with the periodic photonic crystal structure, proving the optical coupling between the nanocapsule and the PCS. Besides, compared with the case of flat Si_3N_4 film, the number of hot spots on the PCS has increased and the overall hot spot

DOI: 10.1021/acssensors.6b00586
ACS Sens. 2017, 2, 346–353

density is enhanced as well. In the simulation, the overall SERS EF increases by 73%. In practice, most of the SERS signals of the analyte come from a few extremely strong hot spots. This case is especially true for a few molecules or even single molecule detection. Therefore, we only count the hot spots that have E^4 enhancement bigger than 10^4 in the plotted region. The results are much more promising: the total hot spot volume increases 3.8 times and the corresponding SERS EF increases 4.8 times, which match our experimental results in quantity.

With the understanding that the enhancement is due to the plasmonic−photonic interactions, next, we investigated the electrokinetic focusing of molecules to the plasmonic nanocapsules under ac electric fields, the second mechanism we employed to enhance SERS detection. To study the sole contribution of electrokinetics, we conducted experiments on a planar ITO glass substrate by dispersing and assembling the nanocapsules on pairs of parallel microelectrodes (gap size ∼20 μm). The nanocapsules were assembled on the edges of the microelectrodes and aligned along the direction of the electric fields at 700 kHz and 20 V. Next, we carefully dispersed analyte molecules, such as adenine (14 μL, 10 μM), and collected Raman spectra continuously from the nanocapsules for a total of ∼480 s, where the ac field (70 kHz to 400 kHz at 20 V) was applied for ∼180 s. Characteristic Raman peaks of analyte molecules were evaluated, i.e., at 736 cm^{-1} for adenine molecules, to reveal the time-dependent enrichment of molecules by the *E*-field. The full spectrum of 10 μM adenine is shown in Figure 9e. It is found that the overall intensity of Raman signals increases monotonically before reaching a plateau in an *E*-field (Figure 7a). The increase of the signals depends on the molecular species and AC frequency (Figure 7), For instance, for adenine, the highest signal increase ∼20% at 70 kHz (Figure 7a).

The enhancement can be attributed to the manipulation and focusing of molecules by ac electric fields, the so-called electrokinetic effects. Distinct from the previous works,[37] the analyte molecules are focused to the SERS-sensitive Ag NPs on the surface of insulating nanocapsules, whereas no *E*-field is directly applied. To understand the effect, we designed two sets of experiments: one was conducted on nanocapsules attached to the edges of the microelectrodes (Figure 8f) and the other on nanocapsules positioned in the center between parallel microelectrodes of 100 μm gap with minimized effects generated from electrodes (Figure 8b). These experiments aim to clarify the molecule focusing mechanisms which may due to the Ag NPs on the surface of nanocapsules or patterned microelectrodes. Fluorescent Cy5 molecules (650 nm absorption, 670 nm emission, 1 μM) were used in this study to clearly determine the motions of molecules in the background suspension, which is difficult to obtain with non-SERS Raman spectroscopy. It is known that alternating current electroosmosis (ACEO) and DEP attraction are the two dominating mechanisms in molecule manipulation by ac *E*-field. ACEO occurs in low-frequency ac *E*-field (<100 kHz in general[38,39]), which generates circulating flows around microelectrodes due to the interaction of the electric double layer and the electric field along the tangential direction. Dielectrophoretic force (F_{DEP}) is due to the interaction between polarized molecules/nanoparticles and external *E*-field. The force is proportional to $E\nabla E$.[34] For positive dielectrophoresis, where the electric polarization of molecules/nanoparticles is stronger than that of the suspension medium, the molecules/nanoparticles can be readily transported toward the highest of the *E*-field gradient (∇E).

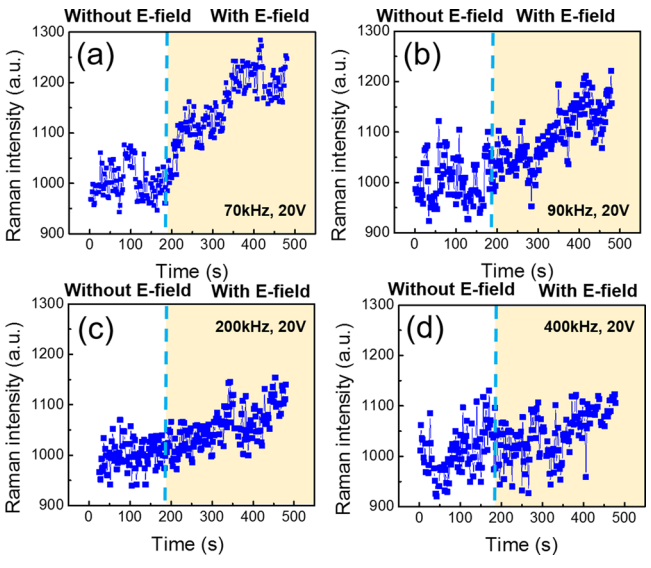

Figure 7. Time-dependent Raman intensity (736 cm^{-1}) of adenine molecules (10 μM) recorded before and after applying an electric field at 20 V and (a) 70 kHz, (b) 90 kHz, (c) 200 kHz, and (d) 400 kHz. The average Raman intensities without electric field are normalized to 1000.

Our tests indicate that both in the vicinity of the microelectrodes (Figure 8h) and on the nanocapsules attached to the microelectrodes (Figure 8g) the concentration of molecules increases with applied ac electric fields (70 kHz, 20 V). The results are consistent with the effect of ACEO flows, which have demonstrated active transportation of nanoparticles, such as quantum dots, to microelectrodes[40] (Figure 8e). To determine if ACEO flow is the sole attribute of molecule focusing, we studied molecule attraction by nanocapsules placed in the center of the microelectrodes, where the ACEO flows are minimized (Figure 8b). We found that the fluorescence of the probing molecules on nanocapsules in the center of microelectrodes still increased remarkably (Figure 8c), while that of the background at a close position remains dormant (Figure 8d). As a result, it can be readily known that even without ACEO flows from the microelectrodes as shown in Figure 8d, the induced electric field at the junctions of Ag NPs can effectively attract molecules to the hot spots. This result is further verified by the numerical simulation using COMSOL 4.4 AC/DC module (Figure 8a).[41] In the junctions of the Ag NPs, the electric field can be substantially increased by 14.6 times of the applied *E* field (the applied *E* field along the *Z* direction is 2×10^5 V/m, and the highest value of enhanced *E* field along the *Z* direction is 2.92×10^6 V/m). This explains the observed attraction of molecules to the surface of nanocapsules, where the induced electric polarization of the Ag NPs can generate ultrahigh *E*-field gradient at their narrow junctions that compel the transport of molecules from suspension to the Ag NPs due to the dielectrophoretic forces (F_{EDP}), $F_{DEP} \propto E\nabla E$.[42,40] Furthermore, the distinct optimal ac frequency for the attraction of different analyte molecules found experimentally as shown in Figure 9 is additional evidence which supports the presence of the DEP effect, where DEP forces highly depend on the electric properties of molecules.

As a result, we experimentally confirmed the unique dual functions of Ag NPs on the surface of nanocapsules, which not

DOI: 10.1021/acssensors.6b00586
ACS Sens. 2017, 2, 346−353

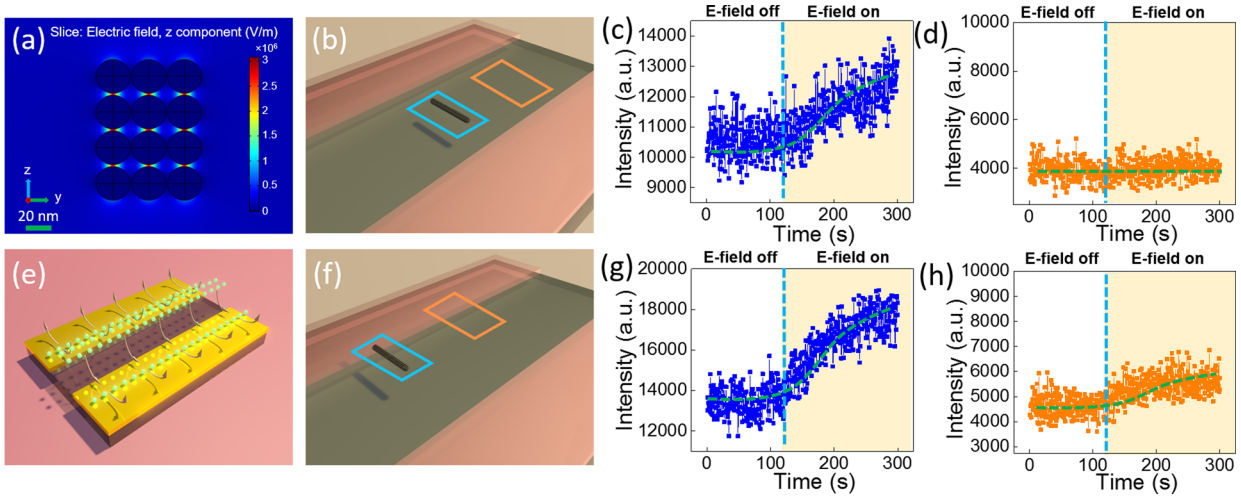

Figure 8. (a) Simulation of a 4 × 3 Ag NP array. The induced *E*-field enhancement is the highest in the junction area (the bar on the right is the magnitude of applied *E* field along the *Z* direction). (b) Schematic of the nanocapsule positioned in the center of the microelectrode gap. We collected the fluorescence signal on the nanocapsule and from the background. (c,d) Time-dependent fluorescence signals on the nanocapsule (blue rectangles) and at the background (orange rectangles), respectively. (e) Schematic shows the ACEO flow which assists in attracting molecules. (f) Schematic of the nanocapsule attached to the edge of the microelectrode. (g,h) Time-dependent fluorescence signals were taken on both nanocapsules (blue rectangles) and background (orange rectangles) at the edge of the microelectrode.

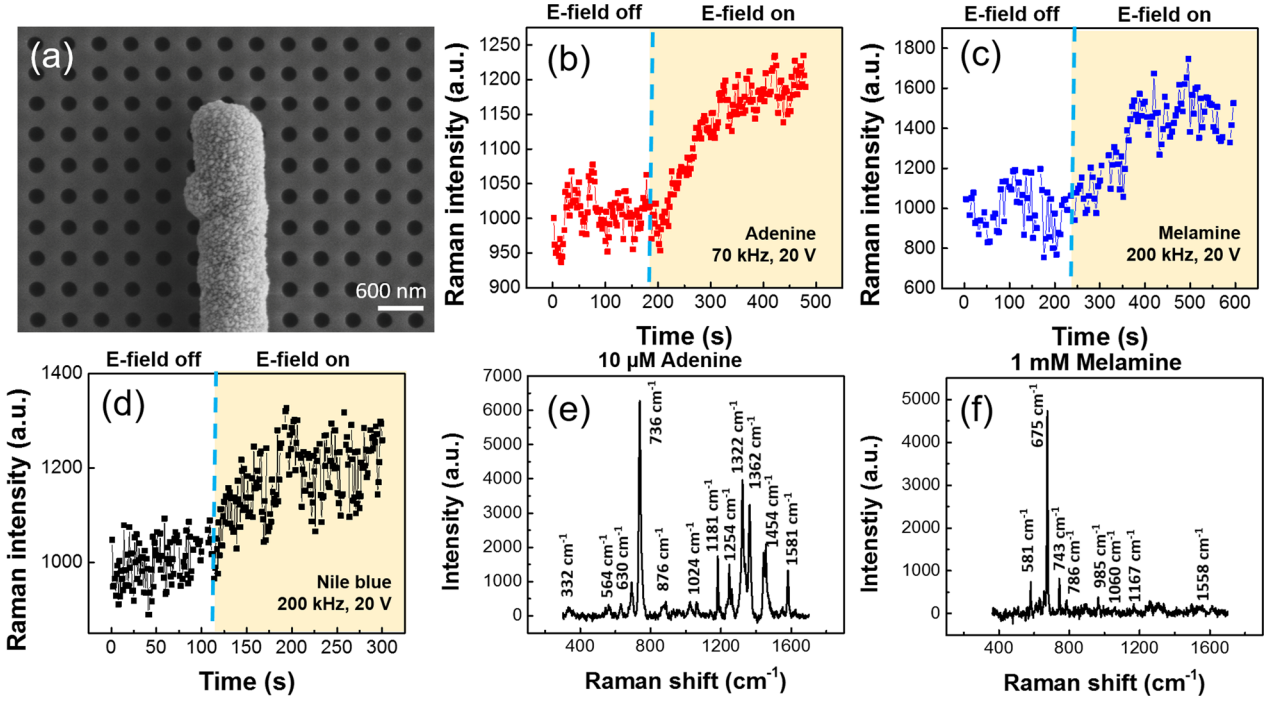

Figure 9. (a) Scanning electron microscopy (SEM) image of assembled nanocapsules on a PCCs integrated with interdigital Au microelectrodes. (b–d) Time-dependent Raman intensity of (b) adenine molecules (10 μM @ 736 cm^{-1}), (c) melamine molecules (1 mM @ 675 cm^{-1}), and (d) Nile blue molecules (100 nM @ 595 cm^{-1}) recorded before and after applying electric fields. Full Raman spectra of (e) adenine (10 μM) and (f) melamine (1 mM).

only provide a high-density layer of plasmonic hot spots for enhancing Raman detection, but also actively enrich molecules to the hot spots in an *E*-field due to the electrokinetic effects.

Finally, we integrated the electrokinetic manipulation with the plasmonic–photonic hybrid devices and demonstrated enhanced molecule detection. The device setup is shown in Figure 1a. Similar to the above experiments on planar ITO glass substrates, first arrays of nanocapsules are assembled on the edges of microelectrodes. They are positioned on the nanoholes of the PCSs. As soon as we apply the electric field, analyte molecules were attracted to the nanocapsules and the SERS signal increased monotonically (Figure 9b–d). At the optimized ac frequency of 200 kHz, 70 kHz, and 200 kHz for Nile blue, adenine, and melamine molecules, respectively, the SERS signal can increase by 19% to 45%. Here the most prominent Raman peaks of analyte molecules were evaluated, i.e., at 595 cm^{-1} for Nile blue, 736 cm^{-1} for adenine, and 675 cm^{-1} for melamine, to quantitatively determine the time-dependent enrichment of molecules by the *E*-field. The full SERS spectra of 10 μM adenine and 1 mM melamine are

DOI: 10.1021/acssensors.6b00586
ACS Sens. 2017, 2, 346–353

shown in Figure 9e,f. Combining the GMR effects from the PCSs, we successfully obtained an overall enhancement of 400−500% robustly in addition to the 3.7×10^8 SERS from the plasmonic nanocapsules. We expect to further improve the EF factor by investigating new designs of PCSs with higher *Q*-factors. We also note that analyte molecules are distributed in 3D volumetric suspensions. At present, our devices are 2D. If changing the schemes from 2D to 3D while keeping the reported features of photonic crystals and integrated plasmonic nanoparticles, we could enhance the detection throughput further.

In summary, we designed and successfully demonstrated an original type of Raman nanosensors by manipulating and integrating chemically synthesized plasmonic nanocapsules on lithographically patterned PCSs with external electric fields. The PCSs can enhance Raman signals by 3 times due to the GMR effect. The patterned microelectrodes not only generate electric fields that align and assemble nanocapsules on the PCSs, but also enable electrokinetic focusing of molecules on the SERS-sensitive surface of nanocapsules. The metallic Ag hot spots on the nanocapsules further enhance molecule attraction to their surfaces due to induced electric fields. The total electrokinetics can boost SERS sensitivity by another 19% to 45%. As a result, an additional enhancement of 400−500% can be obtained on top of the 3.7×10^8 EF from the plasmonic nanocapsules, resulting in a robust 2×10^9 EF. Note that the additional enhancement provided by the GMR from PCSs and electrokinetic focusing are achieved in solution, which is essential for applications of SERS nanosensors in microfluidics. Various biological and environmental interesting molecules, including Nile blue, adenine, and melamine, can be efficiently detected. This work points toward a rational approach in designing future SERS nanosensing devices with ultrahigh sensitivity and efficiency for practical applications.

■ ASSOCIATED CONTENT

Supporting Information

The Supporting Information is available free of charge on the ACS Publications website at DOI: 10.1021/acssensors.6b00586.

Experimental details; simulated reflection spectra of the PCSs (4 designs) (PDF)

■ AUTHOR INFORMATION

Corresponding Authors

*E-mail: wang@eecs.oregonstate.edu.
*E-mail: chenrt@austin.utexas.edu.
*E-mail: dfan@austin.utexas.edu.

ORCID

Zheng Wang: 0000-0002-2143-3847
Donglei Fan: 0000-0002-4724-2483

Author Contributions

¶Chao Liu and Zheng Wang contributed equally to this work.

Author Contributions

D.L.F. and A.W. conceived the project. D.L.F., A.W., and R.T.C. supervised the project. C.L. contributed to nanoparticle synthesis, nanomanipulation, and SERS characterization. Z.W. fabricated PCSs, patterned microelectrodes on PCSs, and conducted RCWA simulations. E.L. and A.W. performed 3D FDTD simulations, and Z.L. performed COMSOL simulations. All authors discussed the results and co-wrote the paper.

Notes

The authors declare no competing financial interest.

■ ACKNOWLEDGMENTS

We thank the support of the National Institutes of Health (NIH) (Grant No. 9R42ES024023-02). D.L.F. thanks Welch Foundation (F-1734) and NSF grants (CMMI 1150767 and EECS 1446489).

■ REFERENCES

(1) Nie, S. M.; Emery, S. R. Probing single molecules and single nanoparticles by surface-enhanced Raman scattering. *Science* **1997**, *275* (5303), 1102−1106.

(2) Kneipp, K.; Wang, Y.; Kneipp, H.; Perelman, L. T.; Itzkan, I.; Dasari, R.; Feld, M. S. Single molecule detection using surface-enhanced Raman scattering (SERS). *Phys. Rev. Lett.* **1997**, *78* (9), 1667−1670.

(3) Long, Y.-T.; Gooding, J. J. Surface-Enhanced Raman Spectroscopy for Sensing—Addressing a Real Challenge in Application. *ACS Sensors* **2016**, *1* (8), 963−963.

(4) Chen, Y.; Zhang, Y.; Pan, F.; Liu, J.; Wang, K.; Zhang, C.; Cheng, S.; Lu, L.; Zhang, W.; Zhang, Z.; Zhi, X.; Zhang, Q.; Alfranca, G.; de la Fuente, J. M.; Chen, D.; Cui, D. Breath Analysis Based on Surface-Enhanced Raman Scattering Sensors Distinguishes Early and Advanced Gastric Cancer Patients from Healthy Persons. *ACS Nano* **2016**, *10* (9), 8169−8179.

(5) Chang, H.; Kang, H.; Ko, E.; Jun, B.-H.; Lee, H.-Y.; Lee, Y.-S.; Jeong, D. H. PSA Detection with Femtomolar Sensitivity and a Broad Dynamic Range Using SERS Nanoprobes and an Area-Scanning Method. *ACS Sensors* **2016**, *1* (6), 645−649.

(6) Zengin, A.; Tamer, U.; Caykara, T. A SERS-Based Sandwich Assay for Ultrasensitive and Selective Detection of Alzheimer's Tau Protein. *Biomacromolecules* **2013**, *14* (9), 3001−3009.

(7) Andreou, C.; Neuschmelting, V.; Tschaharganeh, D.-F.; Huang, C.-H.; Oseledchyk, A.; Iacono, P.; Karabeber, H.; Colen, R. R.; Mannelli, L.; Lowe, S. W.; Kircher, M. F. Imaging of Liver Tumors Using Surface-Enhanced Raman Scattering Nanoparticles. *ACS Nano* **2016**, *10* (5), 5015−5026.

(8) Chou, A.; Jaatinen, E.; Buividas, R.; Seniutinas, G.; Juodkazis, S.; Izake, E. L.; Fredericks, P. M. SERS substrate for detection of explosives. *Nanoscale* **2012**, *4* (23), 7419−7424.

(9) Demeritte, T.; Kanchanapally, R.; Fan, Z.; Singh, A. K.; Senapati, D.; Dubey, M.; Zakar, E.; Ray, P. C. Highly efficient SERS substrate for direct detection of explosive TNT using popcorn-shaped gold nanoparticle-functionalized SWCNT hybrid. *Analyst* **2012**, *137* (21), 5041−5045.

(10) Stuart, D. A.; Biggs, K. B.; Van Duyne, R. P. Surface-enhanced Raman spectroscopy of half-mustard agent. *Analyst* **2006**, *131* (4), 568−572.

(11) Szlag, V. M.; Styles, M. J.; Madison, L. R.; Campos, A. R.; Wagh, B.; Sprouse, D.; Schatz, G. C.; Reineke, T. M.; Haynes, C. L. SERS Detection of Ricin B-Chain via N-Acetyl-Galactosamine Glycopolymers. *ACS Sensors* **2016**, *1* (7), 842−846.

(12) Kang, T.; Yoo, S. M.; Yoon, I.; Lee, S. Y.; Kim, B. Patterned Multiplex Pathogen DNA Detection by Au Particle-on-Wire SERS Sensor. *Nano Lett.* **2010**, *10* (4), 1189−1193.

(13) Barhoumi, A.; Halas, N. J. Label-Free Detection of DNA Hybridization Using Surface Enhanced Raman Spectroscopy. *J. Am. Chem. Soc.* **2010**, *132* (37), 12792−12793.

(14) Bell, S. E. J.; Sirimuthu, N. M. S. Surface-enhanced Raman spectroscopy (SERS) for sub-micromolar detection of DNA/RNA mononucleotides. *J. Am. Chem. Soc.* **2006**, *128* (49), 15580−15581.

(15) Yang, H.; Deng, M.; Ga, S.; Chen, S. H.; Kang, L.; Wang, J. H.; Xin, W. W.; Zhang, T.; You, Z. R.; An, Y.; Wang, J. L.; Cui, D. X. Capillary-driven surface-enhanced Raman scattering (SERS)-based microfluidic chip for abrin detection. *Nanoscale Res. Lett.* **2014**, *9*, 138.

(16) Chen, S. H.; Huang, P.; Wang, Z. H.; Wang, Z.; Swierczewska, M.; Niu, G.; Cui, D. X.; Chen, X. Y. Self-assembly of gold

DOI: 10.1021/acssensors.6b00586
ACS Sens. 2017, 2, 346−353

nanoparticles to silver microspheres as highly efficient 3D SERS substrates. *Nanoscale Res. Lett.* **2013**, *8*, 168.
(17) Stiles, P. L.; Dieringer, J. A.; Shah, N. C.; Van Duyne, R. P. Surface-enhanced Raman spectroscopy. *Annu. Rev. Anal. Chem.* **2008**, *1*, 601−626.
(18) Xu, X.; Kim, K.; Liu, C.; Fan, D. Fabrication and Robotization of Ultrasensitive Plasmonic Nanosensors for Molecule Detection with Raman Scattering. *Sensors* **2015**, *15* (5), 10422.
(19) Wang, A.; Kong, X. Review of Recent Progress of Plasmonic Materials and Nano-Structures for Surface-Enhanced Raman Scattering. *Materials* **2015**, *8* (6), 3024.
(20) Yang, S. K.; Dai, X. M.; Stogin, B. B.; Wong, T. S. Ultrasensitive surface-enhanced Raman scattering detection in common fluids. *Proc. Natl. Acad. Sci. U. S. A.* **2016**, *113* (2), 268−273.
(21) Deegan, R. D.; Bakajin, O.; Dupont, T. F.; Huber, G.; Nagel, S. R.; Witten, T. A. Capillary flow as the cause of ring stains from dried liquid drops. *Nature* **1997**, *389* (6653), 827−829.
(22) Shuai, Y.; Zhao, D.; Singh Chadha, A.; Seo, J.-H.; Yang, H.; Fan, S.; Ma, Z.; Zhou, W. Coupled double-layer Fano resonance photonic crystal filters with lattice-displacement. *Appl. Phys. Lett.* **2013**, *103* (24), 241106.
(23) Wang, S. S.; Magnusson, R. THEORY AND APPLICATIONS OF GUIDED-MODE RESONANCE FILTERS. *Appl. Opt.* **1993**, *32* (14), 2606−2613.
(24) Crozier, K. B.; Lousse, V.; Kilic, O.; Kim, S.; Fan, S.; Solgaard, O. Air-bridged photonic crystal slabs at visible and near-infrared wavelengths. *Phys. Rev. B: Condens. Matter Mater. Phys.* **2006**, *73* (11), 115126.
(25) Tabatabaei, M.; Najiminaini, M.; Davieau, K.; Kaminska, B.; Singh, M. R.; Carson, J. J. L.; Lagugne-Labarthet, F. Tunable 3D Plasmonic Cavity Nanosensors for Surface-Enhanced Raman Spectroscopy with Sub-femtomolar Limit of Detection. *ACS Photonics* **2015**, *2* (6), 752−759.
(26) Le Ru, E.; Etchegoin, P. *Principles of Surface-Enhanced Raman Spectroscopy: and related plasmonic effects*; Elsevier, 2008.
(27) Li, J. J.; Fattal, D.; Li, Z. Y. Plasmonic optical antennas on dielectric gratings with high field enhancement for surface enhanced Raman spectroscopy. *Appl. Phys. Lett.* **2009**, *94* (26), 263114.
(28) Kim, S. M.; Zhang, W.; Cunningham, B. T. Coupling discrete metal nanoparticles to photonic crystal surface resonant modes and application to Raman spectroscopy. *Opt. Express* **2010**, *18* (5), 4300−4309.
(29) Xu, X. B.; Hasan, D. H.; Wang, L.; Chakravarty, S.; Chen, R. T.; Fan, D. L.; Wang, A. X. Guided-mode-resonance-coupled plasmonic-active SiO_2 nanotubes for surface enhanced Raman spectroscopy. *Appl. Phys. Lett.* **2012**, *100* (19), 191114.
(30) Xu, X. B.; Kim, K.; Li, H. F.; Fan, D. L. Ordered Arrays of Raman Nanosensors for Ultrasensitive and Location Predictable Biochemical Detection. *Adv. Mater.* **2012**, *24* (40), 5457−5463.
(31) Xu, X. B.; Kim, K.; Fan, D. L. Tunable Release of Multiplex Biochemicals by Plasmonically Active Rotary Nanomotors. *Angew. Chem., Int. Ed.* **2015**, *54* (8), 2525−2529.
(32) Whitney, T. M.; Jiang, J. S.; Searson, P. C.; Chien, C. L. Fabrication and Magnetic-Properties of Arrays of Metallic Nanowires. *Science* **1993**, *261* (5126), 1316−1319.
(33) Fan, D. L.; Zhu, F. Q.; Cammarata, R. C.; Chien, C. L. Electric tweezers. *Nano Today* **2011**, *6* (4), 339−354.
(34) Jones, T. B. *Electromechanics of particles*; Cambridge University Press: Cambridge; New York, 1995; p *xxii*, 265 p.
(35) Fan, D. L.; Zhu, F. Q.; Cammarata, R. C.; Chien, C. L. Manipulation of nanowires in suspension by ac electric fields. *Appl. Phys. Lett.* **2004**, *85* (18), 4175−4177.
(36) Liu, V.; Fan, S. S 4: A free electromagnetic solver for layered periodic structures. *Comput. Phys. Commun.* **2012**, *183* (10), 2233−2244.
(37) Cherukulappurath, S.; Lee, S. H.; Campos, A.; Haynes, C. L.; Oh, S.-H. Rapid and sensitive in situ SERS detection using dielectrophoresis. *Chem. Mater.* **2014**, *26* (7), 2445−2452.
(38) Green, N. G.; Ramos, A.; Gonzalez, A.; Morgan, H.; Castellanos, A. Fluid flow induced by nonuniform ac electric fields in electrolytes on microelectrodes. I. Experimental measurements. *Phys. Rev. E: Stat. Phys., Plasmas, Fluids, Relat. Interdiscip. Top.* **2000**, *61* (4), 4011−4018.
(39) Wong, P. K.; Wang, T. H.; Deval, J. H.; Ho, C. M. Electrokinetics in micro devices for biotechnology applications. *IEEE-ASME Trans. Mechatron.* **2004**, *9* (2), 366−376.
(40) Liu, C.; Kim, K.; Fan, D. L. Location deterministic biosensing from quantum-dot-nanowire assemblies. *Appl. Phys. Lett.* **2014**, *105* (8), 083123.
(41) Here hemispherical Ag NPs (4 × 3) with junctions of 1.8 nm and diameter of 26 nm are arranged on a fused glass substrate in an ac *E*-field of 2×10^5 V/m in the *Z* direction.
(42) Cheng, I.-F.; Chen, T.-Y.; Lu, R.-J.; Wu, H.-W. Rapid identification of bacteria utilizing amplified dielectrophoretic force-assisted nanoparticle-induced surface-enhanced Raman spectroscopy. *Nanoscale Res. Lett.* **2014**, *9* (1), 324.

DOI: 10.1021/acssensors.6b00586
ACS Sens. 2017, 2, 346−353

Electrokinetic Manipulation Integrated Plasmonic-Photonic Hybrid Raman Nanosensors with Dually Enhanced sensitivity

Chao Liu,[†¶] Zheng Wang,[†‡¶] Erwen Li,[§] Zexi Liang,[†] Swapnajit Chakravarty,[⁄⁄] Xiaochuan Xu,[⁄⁄]

Alan X. Wang,[*§] Ray T. Chen,[*†‡] and Donglei Fan[*†⊥#]

[¶]*These authors contributed equally to this work*

†Materials Science and Engineering Program, Texas Materials Institute and ⊥Department of Mechanical Engineering, The University of Texas at Austin, Austin, Texas 78712, United States

‡Department of Electrical and Computer Engineering, The University of Texas at Austin, 10100 Burnet Road, MER 160, Austin, Texas 78758, United States

§ School of Electrical Engineering and Computer Science, Oregon State University, Corvallis, Oregon 97331, United States

⁄⁄ Omega Optics, Inc., 8500 Shoal Creek Boulevard, Building 4, Suite 200, Austin, Texas 78757, United States

#Nova Minds LLC, 9535 Ketona Cv., Austin, Texas 78759, United States

KEYWORDS: surface-enhanced Raman scattering, photonic crystal, guided-mode resonance, electrokinetics, Nanomanipulation, Raman nanosensor, Biosensing, Microfluidics

Table of Content

Fabrication of Au-cored nanocapsules:

The fabrication of nanocapsules starts with the electrochemical deposition of Au nanorods into anodic aluminum oxide (AAO) templates with copper layers evaporated on the backsides of the templates. Here, the Au electrolyte we used is commercially available cyanide based solution (434 HS RTU, Technic Inc.). The diameter of the nanorods can be controlled by the pore size of the AAO templates from tens of nanometers to 400 nm, and the length of the Au nanowires depends on the total amount of electric charge passing through the circuit. After dissolving the AAO template in 2 M NaOH solution, the nanowires are resuspended and sonicated in ethanol and deionized (D. I.) water alternatively before redispersed in D. I. water. Over 10^9 nanowires can be fabricated at a time with an average length of 9.1 μm and diameter of 298 nm as shown in Fig. 4b. Next, a silica layer of 180 nm in thickness is synthesized on the surface of Au nanorods via hydrolysis of tetraethyl orthosilicate (TEOS, 0.8 mL, Alfa Aesar, 99.999+%) in ammonia (0.2 mL, Fisher Scientific, Certified A.C.S. Plus), ethanol (3 mL, Pharmco-aaper, ACS/USP grade), and D. I. water (1.8 mL) mixture solution under sonication for 1 hour. Finally, Ag NPs are synthesized on the surface of silica layer by mixing Au@SiO_2 nanowires with freshly prepared 500 μL, 0.06 M silver nitrate ($AgNO_3$, ACROS Organics, 99.85%), and 250 μL, 0.12 M ammonia and stirring for 1 hour before adding polyvinylpyrrolidone (PVP, 10 mL of 2.5×10^{-5} M in ethanol, Sigma-Aldrich, M_w=40000) to promote the growth of Ag NPs at 70 ^oC. After 7-hour reaction, dense Ag NPs are obtained on the entire surface of the nanocapsules as shown in Fig. 4d. Here, The size of Ag NPs and hot spot junctions here are 26 ± 5 nm and 1.8 ± 0.4 nm (we only consider junctions of <2 nm as hot spots[1]), respectively. We note that nanocapules fabricated with this approach have slight variations among different batches, *i.e.* with a repeated experiment, we obtained nanocapsules

with Ag nanoparticles of 29.6 ± 10 nm in size and 1.5 ± 0.3 nm in hot spot junction, which demonstrates the controllability of the synthesis.

Raman Testing Setup and Details

The nanocapsules which were suspended in the ethanol solution were first dispersed on the PCS within a Polydimethylsiloxane (PDMS) well. After the evaporation of the ethanol solution, 20 μL of 100 nM Nile blue solution was dispersed into the well and covered with a cover glass. After 10 mins incubation, the PCS with the nanocapsules on it was flipped over and fixed on a customized Raman microscope. Due to the interfacial force between the nanocapsules and the PCS, the nanocapsules attached to PCS firmly. The cover glass effectively sealed the PDMS well, and thus prevented the leaking of Nile blue solution from the well. A 633 nm Helium-Neon laser (randomly polarized, Research Electro-Optics, Inc.) was used to illuminate the nanocapsules via a 20X objective lens (NA: 0.45, Olympus MPLFLN20XBD). The resulting signals were collected from the same objective, filtered by a 633 nm edge filter (633 nm RazorEdge long pass edge filter, Semrock, Inc.), and analyzed by a high sensitive spectrometer (Acton 2500, Princeton Instruments, Inc).

Experimental details for imaging the molecule attraction process

The nanocapsules which suspended in ethanol solution were dispersed in a Polydimethylsiloxane (PDMS) well assembled on ITO parallel microelectrodes (gap size: 102 μm). After the evaporation of the ethanol solution, the nanocapsules can attach to the substrate firmly. Next 20 μL of 1 μM Cy5 labeled biotin solution was dispersed into the PDMS well and covered with a glass slide. An inverted microscope (IX 71, Olympus, Inc.) equipped with a spectrograph (Acton 2500, Princeton Instruments, Inc.), a high-speed ultrasensitive charge-coupled device (CCD) camera (ProEm 512B, Princeton Instruments, Inc.), and a

photoluminescence illumination system (Prior Scientific, Inc.) was employed to collect the spectra and images of Cy5 molecules. A 605 nm band pass filter and a 633 nm edge filter were used. The time-dependent fluorescence spectra of Cy5 molecules were recorded continuously with an exposure time of 0.6 s. The intensity of the fluorescence emission peak at 670 nm was used for analysis.

SERS Enhancement Factor Estimation of Nanocapsules:

We estimated SERS enhancement factor (EF) of the nanocapsules. As aforementioned, the fabrication of nanocapsules is controllable with slight variations among different batches. We characterized nanocapsules with SEM before conducting experiments for EF estimation. The nanocapsules in the test have diameter of 29.6 ± 10 nm, average hot spot junction of 1.5 ± 0.3 nm, and density of hot spots of 787 hotspots/ μm^2. The characterization was done by following the same method that have been employed by various groups[1, 2].

We used 1, 2-bis(2-pyridyl)ethylene (BPE), a type of non-resonant molecules, as the test reagent to determine the EF. Note that non-resonant molecules can provide better accuracy for the estimation of EF of plasmonic substrates. The SERS EF was calculated by following a commonly used method as given below[2]:

$$\boldsymbol{EF = \frac{I_{SERS}/N_{SERS}}{I_{RS}/N_{RS}}} \qquad \textbf{Eq. S1}$$

where N_{SERS} is the average number of adsorbed molecules in the scattering volume of the SERS hot spots. I_{SERS} is the corresponding SERS intensity; N_{RS} is the average number of molecules in the scattering volume (V_{scat}) in suspension for the Raman (non SERS) measurement, I_{RS} is the corresponding Raman intensity.

The values of I_{RS} were obtained from 0.1 M BPE dissolved in ethanol. A laser power of 1 mW (633 nm, randomly polarized, Research Electro-Optics, Inc.) was chosen and was fully focused into the BPE solution via a 20× objective (NA: 0.45, Olympus MPLFLN20XBD). A Raman spectrum with an intensity (I_{RS}) of 273 counts (at 1200 cm^{-1}) was obtained. The 1200 cm^{-1} peak was chosen due to its great separation from other Raman peaks.

N_{RS} is given by $N_{RS} = CV_{scat}N_A$, where C is the concentration of the analyte molecules which is the concentration of BPE solution (0.1 M), V_{scat} is the scattering volume which contributes to the Raman intensity, N_A is Avogadro's number. V_{scat} is determined by $V_{scat} = A_{obj}H_{obj}$, where $A_{obj} = \pi R^2$ is the area of the laser spot from the 20× objective, here R is the laser spot size which was measured as 4.5 μm; H_{obj} is the effective height of the detection volume of BPE. The value of H_{obj} was determined by using the method reported previously.[3] In brief, the measurement was carried out by moving a silicon <100> wafer with 1 μm increment by using the piezoelectric stage controller (ASIimager) through the focal plane of the objective and collecting the intensity of Si Raman signal at 520 cm^{-1} at each point. $H_{obj} = 45.2\ \mu m$ was obtained by integrating the intensity of Raman signal with distance and then dividing by the highest measured signal. By using this method, V_{scat} was determined to be $V_{scat} = A_{obj}H_{obj} = \pi(\frac{4.5}{2})^2 \times 45.2 = 718.5\ (\mu m^3)$.

Therefore, the total number of molecules (NRS) can be calculated as:

$$N_{RS} = CV_{scat}N_A = 0.1\ mol/L \times 718.5\ \mu m^3 \times 6.02 \times 10^{23}\ molecules/mol$$
$$= 4.33 \times 10^{10}\ molecules$$

To determine the value of I_{SERS}, we dispersed nanocapsules on a glass substrate and dried them in air, and then incubated them in 1 mM BPE ethanol solution for 10 min. The

nanocapsules were then rinsed with pure ethanol to remove excess molecules and dried in air. Since the nanocapsules are cylinders with curvature (660 nm in diameter), we approximated the effective area excited by the laser (spot size 4.5 μm) as 4.5 μm ×0.2 μm= 0.9 μm^2. Under the same experimental condition as described above, we obtained an I_{SERS} of 30742 counts (at 1200 cm^{-1}). Knowing that molecules locating in hot spots (3.375 nm^3 volume of 1.5 ± 0.3 nm narrow junction) contribute to most of the obtained SERS signals. There are approximately 18.75 molecules/hot spot for a close packed monolayer of BPE (3 Å × 6 Å × 10 Å/molecule)[2c]. Also the average hot spot density is 787 hotspots/μm^2. Therefore, the average number of molecules in the scattering volume for the SERS experiments is:

$$N_{SERS} = 0.9\,\mu m^2 \times 787\ \ hotspots/\mu m^2 \times\ 18.75\, molecules/hotspot = 13280.625$$

Then,

$$EF = \frac{I_{SERS}/N_{SERS}}{I_{RS}/N_{RS}} = \frac{30742/13280.625}{273/(4.33 \times 10^{10})} = 3.7 \times 10^8$$

This value is slightly different from previous work[1] and can be attributed to the following factors:

1. The synthesized nanocapsules have slight variations in Ag nanoparticles from previous samples. It could because even though the synthesis processes are similar, the structures of nanocapsules are slightly different. Our present nanocapsules only have Au nanowires as the cores. While, the previous nanocapsules have cores made of Ag/Ni nanowires[1].

2. We employed a different Raman laser setup in the test. In this work, 633 nm laser has been used when we conduct all kinds of studies. To be consistent, when determining the EF, we also used the same laser. While, in our previous work, we used 532 nm laser instead. Since Ag

nanoparticles generally have a plasmonic resonance ~450 nm depending on the size[1], the 632 nm laser used here are further away from the resonance peak compared with the 532 nm laser, which leads to the lower EF values in measurement.

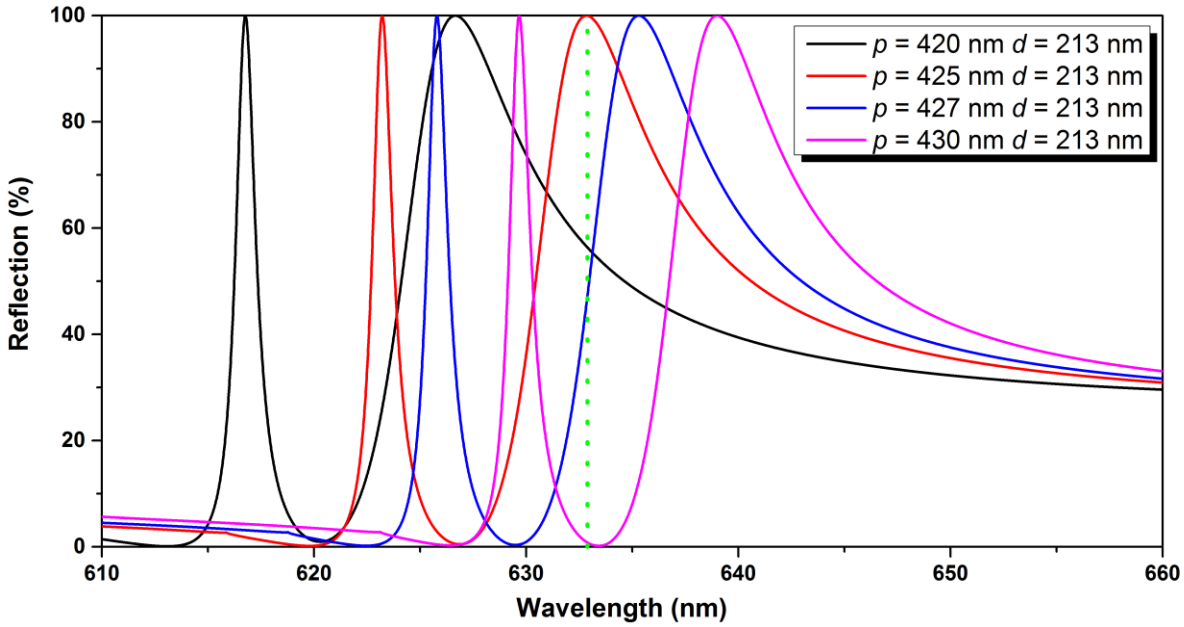

Figure S1 Simulated reflection spectra of the four designs of PCSs. The green dot line represents the excitation laser wavelength at 633 nm.

References

1. Xu, X. B.; Kim, K.; Li, H. F.; Fan, D. L., Ordered Arrays of Raman Nanosensors for Ultrasensitive and Location Predictable Biochemical Detection. Adv Mater 2012, 24 (40), 5457-5463.
2. (a) Le Ru, E. C.; Blackie, E.; Meyer, M.; Etchegoin, P. G., Surface enhanced Raman scattering enhancement factors: a comprehensive study. J Phys Chem C 2007, 111 (37), 13794-13803; (b) Schmidt, M. S.; Hubner, J.; Boisen, A., Large Area Fabrication of Leaning Silicon Nanopillars for Surface Enhanced Raman Spectroscopy. Adv Mater 2012, 24 (10), Op11-Op18; (c) Hu, M.; Ou, F. S.; Wu, W.; Naumov, I.; Li, X. M.; Bratkovsky, A. M.; Williams, R. S.; Li, Z. Y., Gold Nanofingers for Molecule Trapping and Detection. J. Am. Chem. Soc 2010, 132 (37), 12820-12822.
3. Smythe, E. J.; Dickey, M. D.; Bao, J. M.; Whitesides, G. M.; Capasso, F., Optical Antenna Arrays on a Fiber Facet for in Situ Surface-Enhanced Raman Scattering Detection. Nano Lett 2009, 9 (3), 1132-1138.